High-Resolution Surface Analysis on Aluminum Oxide-Coated $Li_{1.2}Mn_{0.55}Ni_{0.15}Co_{0.1}O_2$ with Improved Capacity Retention

Nadine Dannehl,[†,‡,*] Sven Ole Steinmüller,[‡,∥] Dorothée Vinga Szabó,[‡,§,⊥] Mathias Pein,[†] Florian Sigel,[‡] Lars Esmezjan,[‡] Ulrich Hasenkox,[†] Björn Schwarz,[‡] Sylvio Indris,[‡] and Helmut Ehrenberg[‡]

[†]Robert Bosch GmbH, Robert Bosch Campus 1, 71272 Renningen, Germany

[‡]Karlsruhe Institute of Technology, Institute for Applied Materials, Hermann von Helmholtz Platz 1, 76344 Eggenstein Leopoldshafen, Germany

[§]Karlsruhe Institute of Technology, Karlsruhe Nano Micro Facility, Hermann von Helmholtz Platz 1, 76344 Eggenstein Leopoldshafen, Germany

[⊥]Karlsruhe Institute of Technology, Institute of Nanotechnology, Hermann von Helmholtz Platz 1, 76344 Eggenstein Leopoldshafen, Germany

ABSTRACT: Thin alumina coatings on Li rich nickel cobalt manganese oxide (Li rich NCM) particles used as cathode material in Li ion batteries can improve the capacity retention during cycling. However, the underlying mechanisms are still not fully understood. It is crucial to determine the degree of coverage of the particle's coating on various length scales from micrometer to nanometer and to link it to the electrochemical properties. Alumina coatings applied on Li rich NCM by atomic layer deposition or by chemical solution deposition were examined. The degree of coverage and the morphology of the particle coatings were investigated by time of flight secondary ion mass spectrometry (ToF SIMS), scanning electron microscopy, elemental analysis using inductively coupled plasma optical emission spectrometry, and scanning/transmission electron microscopy. ToF SIMS allows investigating the coverage of a coating on large length scales with high lateral resolution and a surface sensitivity of a few nanometers. Regardless of the chosen coating route, analytical investigations revealed that the powder particles were not covered by a fully closed and homogenous alumina film. This study shows that a fully dense coating layer is not necessary to achieve an improvement in capacity retention. The results indicate that rather the coating process itself likely causes the improvement of the capacity retention and increases the initial capacity.

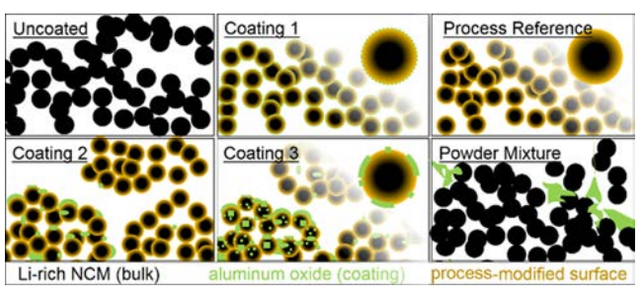

KEYWORDS: *Li ion battery, cathode, chemical solution deposition (CSD) coatings, atomic layer deposition (ALD), Li rich NCM, aluminum oxide cathode coatings, time of flight secondary ion mass spectrometry (ToF SIMS)*

1. INTRODUCTION

Mn and Li rich transition metal layered oxides Li($Li_xMn_{1-x-y-z}Ni_yCo_z$)O_2 (e.g., $Li_{1.2}Mn_{0.55}Ni_{0.15}Co_{0.1}O_2$ as used in this study) are a very promising class of cathode materials for Li ion batteries due to their high specific discharge capacity and energy. Nevertheless, a large capacity and voltage fade occur for these cathode materials during electrochemical cycling.[1] According to Xu et al.,[2] Wen et al.,[3] Park et al.,[4] and Zhang et al.,[5] thin inorganic coatings on the cathode particles made of aluminum oxide are supposed to prevent the capacity fading of Li Rich NCM. Yet the underlying stabilization mechanism is not fully understood. A dense coating is said to be crucial to avoid reactions between electrolyte and cathode material as well as to improve the capacity retention.[2] The investigations of the coating influence on the electrochemical degradation process require information about the coverage, morphology, and atomic structure. Promising alumina coating processes already described in the literature[2−5] were chosen and applied on the cathode active material $Li_{1.2}Mn_{0.55}Ni_{0.15}Co_{0.1}O_2$. The obtained samples were investigated with surface analysis methods to get a high level of lateral and depth resolution of the applied coating. To increase the sensitivity for surface induced degradation effects, Li rich NCM with a high surface area and thus small particle size was synthesized. To avoid reactions of the electrolyte with the cathode material and to improve the capacity retention, a dense coating film completely covering the surface of the cathode material is assumed to be required. The analytical

approach to distinguish between a thin and dense surface layer and a just partial island covered cathode material is very challenging and not yet reported in literature for cathode particle coatings. Scanning electron microscopy (SEM) with energy dispersive X ray spectroscopy (EDX) reveals the distribution of a coating material on a micrometer scale. Still, the limitation is the insufficient surface sensitivity of EDX due to a large contribution from the bulk to the measurement signal. This prevents to quantify the surface coverage of a coating with nanometer resolution. Thus, it would not be clear whether the Al is located on the surface or in the bulk. Scanning/transmission electron microscopy (S/TEM) imaging combined with EDX is able to reveal the morphology and crystal structure of thin coatings, as well as chemical composition of the area under investigation, but it is restricted to a very local scale and therefore cannot provide statistically relevant data for the material. X ray photoelectron spectros copy can provide information about the surface composition but lacks lateral spatial resolution. All mentioned analytical methods are therefore not able to examine the coverage with the intended lateral spatial resolution of several micrometers combined with a nanometer depth resolution.

In this work, it is shown that it is possible to overcome most of these restrictions by using time of flight secondary ion mass spectrometry (ToF SIMS) with different detection modes. Starting with a model system for the calibration of the surface sensitivity for the ToF SIMS measurements, it is possible to characterize thin coatings of a micrometer sized surface area with nanometer information depth and statistically relevant results. Silicon wafers coated with various well defined thicknesses of alumina coatings prepared by atomic layer deposition (ALD) were used as a reference system. By comparison of the model system and the material of interest, a reliable method for the estimation of the surface coating thickness of three dimensional shaped particles is presented. It is not possible to perform depth profiling directly due to electrostatic charging of the investigated loose particles. Combined information from S/TEM with EDX can clarify the degree of coverage by a coating with nanometer resolution.

In addition, the specific discharge capacity of the sample prepared by chemical solution deposition (CSD) was compared to that of reference samples to distinguish between the contributions from the wet coating process itself and the influence of aluminum oxide present in the material system. Taking the results of different methods into account, a detailed understanding of the influence of three different surface modifications and reference samples on the electrochemical properties is presented.

2. MATERIALS AND METHODS

2.1. Material Preparation. $Li_{1.2}Mn_{0.55}Ni_{0.15}Co_{0.1}O_2$ was synthe sized using a sol−gel method with acetate precursors (Co(II)Ac·$4H_2O$, purity ≥ 98% Alfa Aesar; Mn(II)Ac·$4H_2O$, ≥ 99% Aldrich, Ni(II)Ac·$4H_2O$ ≥ 98%, Alfa Aesar, LiAc·$2H_2O$ Alfa Aesar ≥ 99%) and citric acid (VWR chemicals, purity > 99.99%) as a chelating agent dissolved in ultrapure water. Precursor contaminations contain no aluminum and thus do not influence the following experiments. After dissolving stoichiometric amounts of the acetate precursors overnight, the pH was adjusted to 7.5 by careful addition of 25% ammonia solution. The solution was evaporated at 80 °C until a greyish viscous gel was obtained, which was dried overnight at 125 °C on a hot plate in air and afterward for 24 h at 120 °C in a muffle oven in air. Then, the precursor was precalcined at 450 °C in air for 6 h, mixed in a mortar, and calcined at 900 °C in air for 12 h. The powders were ground in a planetary mill using 3 mm ZrO_2 milling balls and acetone for 30 min at 500 rpm. The target elemental composition of this material has been analytically validated by inductively coupled plasma optical emission spectrometry (ICP OES), as shown in Table S1.

2.1.1. Preparation of Different Surface Modifications and Reference Samples. All coating procedures described in this paper are based on promising literature data, which propose improved capacity retention due to aluminum oxide coatings.[2−5]

The as synthesized Li rich NCM without any ball milling has a specific surface area of 2 m^2/g.

Wet coating (named CSD for chemical solution deposition): Two different materials were used as starting material for the wet coating. Li rich NCM with a specific surface area of 4 m^2/g was used in a previous study. This material experienced a very short milling duration. The particles were processed with coating amounts of 1, 2, and 4 wt % following the procedure reported by Xu et al.,[2] because these concentrations lead to improved capacity retention.[2−4] The previous studies showed that only the concentration of 1 wt % had the tendency to stabilize the capacity of the price of a small loss of initial capacity, similar to the results reported by Xu et al.[2] To increase the sensitivity of surface dependent degradation processes by a higher specific surface area (14 m^2/g), a longer duration of ball milling was applied according to the description given above. Following Han et al.,[6] a target coating amount of 0.5 wt % alumina was used. Han et al.[6] showed increased capacity retention for an alumina coating on $LiNi_{0.5}Co_{0.2}Mn_{0.3}O_2$ cathode particles with very low loss of initial capacity. For the CSD sample used in this study, $Al(NO_3)_3·9H_2O$ (Fluka) was dissolved in ethanol and Li rich NCM was added so that the final product contained 0.5 wt % alumina. The solvent was evaporated under continuous stirring at 80 °C, and the powder was dried and annealed at 500 °C for 4 h. This process is similar to the synthesis route described by Park et al.[4]

2.1.2. Coating by Atomic Layer Deposition. Li rich NCM powders were filled into a powder coating unit of a forced flow atomic layer deposition reactor (R 200 Advanced ALD reactor by Picosun), heated, and alternatingly dosed with water vapor, nitrogen, trimethylaluminum (TMA), and nitrogen again for several coating cycles. The process was adjusted in such a way that 2−3 nm of coating thickness on a reference Si wafer was achieved. This target thickness was chosen following procedures described by Zhang et al.[7] The ALD S ("S" stands for shaking) coating was performed by the company Picosun Finland using 250 °C as reactor temperature. To get a high enough dose, both precursors were pulsed 160 times in a row and the available surface area was maximized by vibrating the powder coating unit during the deposition. The coating process started with alternating dosing of TMA (160 pulses, 120 sccm, 0.1 s for each pulse, 2 s purge between pulses), 320 s purge, water (160 pulses, 150 sccm, 0.1 s pulse for each pulse, 2 s purge between pulses), and 320 s purge, repeatedly, 15 times. The ALD NS ("NS" stands for no shaking) coating was performed at Karlsruhe Institute of Technology, Institute of Nanotechnology using 130 °C as reactor temperature. Again, a forced flow atomic layer deposition reactor equipped with a powder coating unit was used. No shaking of the powder was done during the process of the ALD NS sample coating. In a first step five, 0.1 s pulses of water (200 sccm) were used to saturate the surface with water. After 4 s purging, the coating process started with alternating dosing of TMA (150 sccm, 0.1 s pulse), 6 s purge, water (200 sccm, 0.1 s pulse), and 6 s purge, repeatedly, 13 times.

2.1.3. Reference Materials. For the powder mixture reference sample ("Mix"), aluminum oxide was produced by the dissolution of $Al(NO_3)_3·9H_2O$ in ethanol without presence of Li rich NCM, followed by the evaporation of the solvent at 80 °C, drying of the powder, and annealing at 500 °C for 4 h. This is the same procedure as that for the CSD sample but without the Li rich NCM. The aluminum oxide was ground using a mortar, and 0.5 wt % of this as synthesized powder was mixed together with the Li rich NCM base cathode material. For the process reference sample ("Proc"), the wet coating process of the base Li rich NCM material was performed

without using the $Al(NO_3)_3$ precursor. Table 1 gives an overview of the used samples.

Table 1. Sample Overview

sample name	preparation
uncoated	as-prepared powder (2 m^2/g) and ball-milled pristine powder (14 m^2/g, starting material for the samples ALD-NS, ALD-S, CSD, Proc, and Mix)
ALD-NS	ALD coating process, no shaking of the powder during coating process
ALD-S	ALD coating process, shaking of the powder during coating process
CSD	chemical solution deposition, wet-coating process
	evaporation of aluminum nitrate in ethanol in presence of the pristine material
	calcination
Proc	process reference
	evaporation of ethanol with presence of the pristine material
	calcination
Mix	powder mixture reference
	evaporation of aluminum nitrate in ethanol without presence of Li-rich NCM
	calcination of this NCM-free Al-containing material
	mixing of this Al-containing material and uncoated Li-rich NCM during slurry preparation

2.2. Electrochemical Testing. Electrochemical testing was conducted in EL cells (ECC Ref type by EL Cell) with a Li reference electrode against Li metal anode and in pouch cell setup using a graphite anode. The cathode composite electrodes were produced by coating a slurry onto Al foil by doctor blading. The slurry contained 87 wt % cathode active material, 7 wt % Solef5130 poly(vinylidene difluoride) (PVDF) binder, and 6 wt % C65 (Timcal) as conductive carbon in *N* methyl 2 pyrrolidone (NMP) with a solid content of 33 wt %. The sheets were uniformly calendered to produce sheets with a porosity of 40 ± 5% and a loading of 4.6 ± 1.6 mg/cm^2. The graphite electrodes were produced by coating a slurry onto copper foil by doctor blading. The slurry contained 97 wt % graphite (50% artificial and 50% natural graphite), 1 wt % carboxymethyl cellulose (Dow Chemical Company), 1 wt % styrene butadiene rubber (Dow Chemical Company), and 1 wt % C65 (Timcal) in water (AnalAR Normapur) with a solid content of 50%. The sheets were uniformly calendered to produce sheets with a porosity of 57 ± 2% and a loading that was adjusted to the cathode loading. The negative to positive capacity ratio used for the full cell studies was adjusted to an excess of anode capacity of 15 ± 1%. For the EL cells, circular electrodes of 17 mm diameter were punched out of the coated aluminum foil and dried in vacuum for at least 720 min at 80 °C. Then, the EL cells were assembled in an argon filled glovebox (<0.1 ppm H_2O, <0.1 ppm O_2) using a 1.55 mm thick glass fiber separator (EL Cell ECC1 01 0012 C) with 350 μL of LP30 electrolyte (BASF, 1 M $LiPF_6$ in ethylene carbonate (EC) and dimethyl carbonate (DMC), 1:1 by volume). For the pouch cells, 22 mm × 22 mm anode and 20 mm × 20 mm cathode electrodes were punched out of the coated foils. The pouch cells were assembled, dried in vacuum for at least 720 min at 80 °C, filled with electrolyte, evacuated, and sealed in the glovebox. The separator used for these cells was Celgard 2500 membrane with 300 μL of LP30 electrolyte.

The cells were charged and discharged in the voltage range of 2.0−4.8 V for the half cells and 2.0−4.7 V for the full cells using a multichannel battery testing instrument (Basytec). A moderate cycling current of 0.1 mA for the half cells (∼C/20) and 0.2 mA (∼C/10) for the full cells was used. A theoretical capacity of 240 mAh/g was used to calculate the cycling current. At least 4 cells of every half cell modification and at least 3 cells for every full cell modification were built to check reproducibility and to estimate the scattering of experimental values. The additional mass of the coating was included in the given specific capacity.

2.3. Characterization. Inductively coupled plasma optical emission spectrometry (ICP OES spectrometer ICap 6300 by Thermo) with chemical pulping by aqua regia and microwave was used for the elemental analysis of the synthesized materials. Specific surface areas were determined by gas adsorption using the Brunauer−Emmett−Teller (BET) model.[8] The isotherms were measured by a Thermo Scientific Surfer Gas Adsorption Porosimeter. The specific surface area was determined from the slope of a two parameter fit in the linear pressure range between $(0.05-0.3)p/p_0$ and $(0.01-0.25)p/p_0$, respectively. The samples were dried in high vacuum (10^{-6} mbar) at 150 °C overnight for preparation. Nitrogen was used as adsorbate. The morphology of the powders was analyzed by a scanning electron microscope Merlin Gemini 2 (Zeiss, Germany) and YPS Schottky thermal field emission cathode using an acceleration voltage of 7 or 10 kV and InLens Detector.

Synchrotron radiation powder diffraction: Ex situ synchrotron radiation powder diffraction (SPD) was performed on samples in 0.5 mm glass capillaries at the High resolution/High throughput Powder Diffraction station BL04 MSPD beamline at ALBA Synchrotron Facility (Barcelona, Spain). A wavelength of 0.4128(3) Å in the 2θ range 1−43° at room temperature was used. Structural analyses by Rietveld refinements[9] were performed using Fullprof program.

Transmission electron microscopy (TEM): TEM was conducted using either a Tecnai F20 ST (FEI, Eindhoven, NL) with a field emission gun operated at 200 kV, equipped with an Orius SC600 CCD camera (Gatan, Pleasanton, CA) and an S UTW EDX Si(Li) detector (EDAX, Mahwah, NJ), or an aberration corrected Titan 80 300 Super Twin (FEI, Eindhoven, NL) instrument with a field emission gun, operated at 300 kV, equipped with a US4000 slow scan CCD camera (Gatan, Pleasanton, CA) and an S UTW Si(Li) EDX detector (EDAX, Mahwah, NJ). EDX line profiles and elemental maps were acquired in STEM mode using drift correction, with a sample tilt of 15 and 20°, respectively. The TEM samples were prepared by dipping a 300 mesh copper grid coated with lacey carbon film directly into the powder. The powders were small (thin) enough to be viewed in transmission mode directly. No additional milling had to be performed for these measurements; therefore, the investigated powder is in the same state as that for the electrochemical measurements.

ToF SIMS was carried out using a ToF SIMS 5 instrument (ION TOF GmbH). Surface spectroscopy was performed with Bi^+ as the primary ion (ion current about 1.5 pA) for secondary ion generation. High mass resolution measurements were performed on two different positions of each powder sample obtaining spectral data and surface images of an area of 2000 × 2000 μm^2 using 200 pixels per 1000 μm. Scan rates of measurements were adjusted to keep the ion dose density below 10^{11} ions/cm^2 per polarity, securing the static SIMS limit of about 10^{12} ions/cm^2, performing positive and negative polarity measurements at identical sample positions. Spectral data were analyzed and exported with SurfaceLab software (version 6.7) of the instrument. Images were gained using the stage raster scan option where several smaller image patches, e.g., 400 × 400 μm^2, were stacked together for large overview scans. All recorded data were flight time corrected using the Advanced ToF Correction feature of the software of the instrument. Brighter colors indicate higher intensity values. High lateral resolution images were recorded by using the "Delayed Extraction" mode of the instrument. Here, areas of 50 μm × 50 μm with a resolution of 256 × 256 pixels were analyzed using Bi^+ as the primary ion for secondary ion generation. The dose density was above the static SIMS limit. For good lateral resolution, signal intensity was accumulated over 100 scans per sample area. Positive polarity measurements were performed at different sample positions, and the measurements were repeated for several different particles. At least two area scans were conducted to check reproducibility of the presented results.

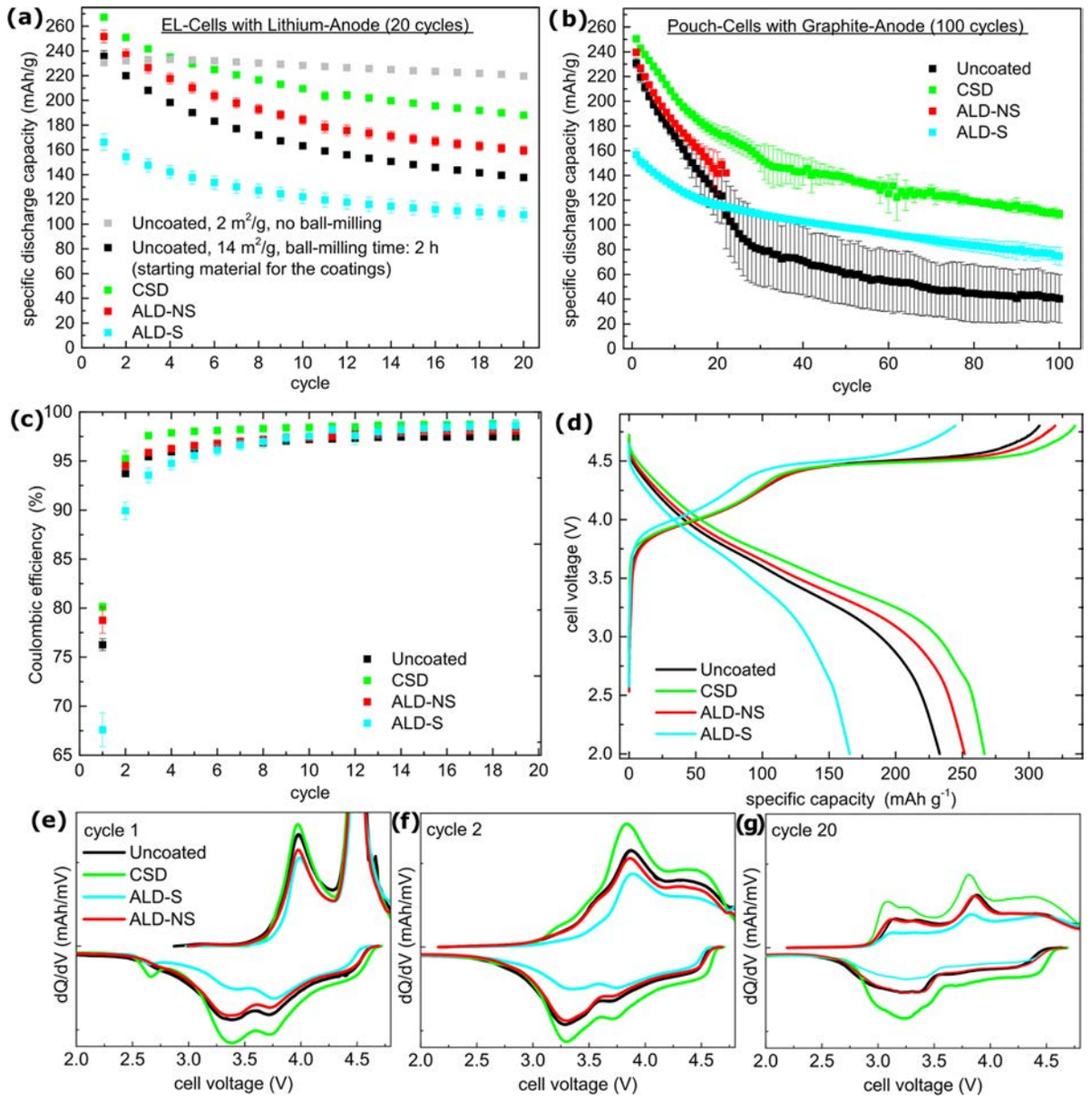

Figure 1. Evolution of discharge capacity of (a) the uncoated cathode material with variation of the specific surface area (ball milling time) and alumina coated Li rich NCM as cathode materials, 20 cycles in half cells, cycled between 2.0 and 4.8 V at a rate of approx. C/20, (b) uncoated and alumina coated Li rich NCM, 100 cycles in full cells, cycled between 2.0 and 4.7 V at a rate of approx. C/10; values represent mean and standard deviation of 4−6 cells; (c−g): Data received from half cell analysis (a); (c) Coulombic efficiency changes with the cycle number of the coated and uncoated samples, average value and standard deviation of 4−6 cells; following data are for one representative cell each: (d) first charge−discharge curves, (e) Corresponding differential charge and discharge plots (two cells are shown for the uncoated material to highlight good reproducibility) for the first cycle, (f) cycle 2, and (g) cycle 20. The color scheme is the same as that in (e).

3. RESULTS AND DISCUSSION

3.1. Electrochemical Examination. The nonmilled powder shows good stability over many cycles, as indicated by the gray curve in Figure 1a. A high specific surface area accelerates the capacity fade with nearly the same initial capacity (black curve). Thus, surface effects play an important role for the degradation mechanisms. To examine surface related degradation processes with a high sensitivity, the sample with the accelerated capacity fade and higher specific surface area was used as starting material for the following experiments.

To identify differences in the initial capacity and capacity retention caused by the various coating processes, the averaged specific discharge capacity versus cycle number of half cells (20 cycles) and full cells (100 cycles) is shown in Figure 1a,b. Individual measurements and the number of cells used for each measurement can be found in the SI (see Figure S1). It is obvious that the initial capacity was increased and capacity retention was improved for the CSD and ALD NS sample. Although Xu et al.[2] and Zhang et al.[5] also report an improved capacity retention, they find decreased initial capacities for the wet and ALD coated samples. Similar to their findings, the ALD S coated samples show an improvement of capacity retention but the initial capacity is decreased by about 30% as compared to that of the uncoated reference sample. The

capacity retention in half cells increased from 58% for the uncoated sample to 70% for the CSD sample.

According to Bloom et al.[10] and Aurbach et al.,[11] the intrinsic voltage fade is a bulk effect that cannot be inhibited by coatings. The results of the dQ/dV analysis also show that the coating has no significant influence on the voltage fade (Figure 1e–g).

The Coulombic efficiency describes the ratio of specific capacity between discharge and the previous charge step. The improvement of the Coulombic efficiency of the ALD NS and CSD modification is shown in Figure 1c. Right from the start, the CSD samples show the highest Coulombic efficiency. In contrast to the Coulombic efficiency of all other samples, ALD S starts with very low Coulombic efficiencies of about 67% and increases with a high slope to the same value as that reached for the CSD samples after 18 cycles. This is likely due to lithiation of the alumina, which consumes lithium and oxygen from the crystal lattice in the first cycles and that would be saturated after a few cycles. $LiAlO_2$ has also a stable phase with low lithium mobility for which Zhang et al.[7] also found indications.

If side reactions during oxidation (charge) were inhibited by a coating, e.g., by preventing contact of the cathode active material surface and the electrolyte, the Coulombic efficiency would increase. For this reason, it is straightforward to interpret a higher Coulombic efficiency as a reduced loss of capacity due to parasitic side reactions like electrolyte oxidation. For Li rich NCM materials, irreversible structural changes take place and also cause an irreversible loss of capacity and influence the Coulombic efficiency.[12]

The first charge–discharge curves shown in Figure 1d exhibit the typical behavior for Li rich NCM with significant differences between the modifications: The first charge curve shows a plateau at 4.5 V belonging to a material activation process. It is typically assigned to irreversible structural changes that include partial lattice oxygen loss from the transition metal oxide surface.[12] During this first charging, the uncoated, ALD NS coated, and CSD samples show the same curve shape until approx. 250 mAh/g. The CSD samples show the longest plateau, followed by ALD NS. The discharge capacity shows the same trend indicated by the length of the discharge plateau. A longer plateau during the first charging goes along with a higher discharge capacity in this experiment.

The variations in the activation processes, i.e., the length of the first charging plateau, result in differences in Coulombic efficiencies: More lithium is intercalated in the first discharge if a higher fraction of material of the coated sample has been activated in the first charge. This results in a higher value of Coulombic efficiency. In accordance with the findings of the charge–discharge curves (Figure 1d), the differences of Coulombic efficiencies (Figure 1c) display a large contribution of modified electrochemical properties of the various powders.

Figure 1d reveals a shoulder at about 2.7 V for the CSD sample. This shoulder is also visible, although less pronounced, for the ALD S sample. It indicates that the Li ions are extracted from a newly formed electrochemical environment with a different potential level. The curve of the ALD S sample has the same shape as that observed for the uncoated sample but in a compressed way along the capacity axis. This indicates that part of the material is electrochemically inactive.

Differential capacity (dQ/dV) of the first cycle is presented in Figure 1e. It shows that the reduction peak corresponding to the oxidation peak occurring at about 3.8 V has smaller integral intensity for the CSD sample (green) but exhibits a reduction process at approx. 3.3 V. This hysteresis is related to the structural changes taking place in this material.[1] Correspond ing to the shoulder for the CSD sample in Figure 1d, a small, sharp reduction peak at about 2.7 V is clearly visible for the CSD sample and indicates a well defined lithiation environ ment. It might be related to surface structural changes induced during the wet chemical surface modification process. Jang et al.[13] report an electrochemical cycling induced spinel for mation in high charge capacity orthorhombic $LiMnO_2$, which provides a sharp reduction peak at about 2.8 V and a broad oxidation peak at about 3.2 V. This indicates that already in the first cycle a contribution of such a spinel phase takes place for the CSD sample. Also, Park et al.[14] reported a structurally integrated layered spinel structure providing a reduction peak at approx. 2.8 V that was assigned to the phase $LiNi_{0.5}Mn_{1.5}O_4$. This phase can be formed by the coating process on the surface of the particles of the active material, as indicated by Wen et al.[3] as well. If this phase transformation just takes place on the particle's surface, more material might be transformed and contribute to the corresponding peak in the differential capacity plot.

As shown in Figure 1f,g, the 2.7 V peak has vanished for the second and subsequent cycles. This is in disagreement with the conclusions from Wen et al.[3] who measured this peak also for further cycles. Probably this spinel like phase vanishes after the first charge due to dissolution into the electrolyte in subsequent cycles. This difference might be caused by the high surface area of the cathode material and low cutoff voltages (2 V) used for the presented experiments, which could increase the tendency of transition metals like manganese to dissolve.

The redox active voltage regime shifts to lower voltages with subsequent cycling. This is commonly attributed to the formation of a spinel like environment.[15]

Comparing the differential capacities of the ALD NS coating (red curve) and the uncoated material (black curve), it is obvious that there are only minor changes and that the electrochemical environment for the lithiation and delithiation remains the same.

3.2. Composition, Crystal Structure, and Microstructure. The diffraction patterns of the as prepared powders measured by synchrotron powder diffraction are shown in Figure 2a. The reflections indicate the formation of a layered structure, which can be indexed on the basis of $LiMO_2$ with M = Mn, Co, and Ni ($R3m$). Additional superstructure reflections between 5.5 and 8.0° were found. These reflections are due to some layered Li_2MnO_3 ($C2/m$) character, which reflect Li and transition metal (TM) ordering in the TM layers, resulting in a superstructure (honeycomb). In contrast to the work of Wen et al.,[3] no spinel phase like $LiMn_2O_4$ or enhanced broadening of the reflections compared with the uncoated reference is detected (see Figure S2 for the Rietveld refinement). A spinel like surface phase with few nanometers of thickness might not provide the necessary long range order for detection by synchrotron powder diffraction. The comparison of the patterns demonstrates that the bulk structure is maintained for all samples. All reflections are ascribable to the above mentioned crystal structure. No aluminum containing phases (e.g., Al_2O_3 or $LiAlO_2$) were measured.

According to the elemental analysis by ICP OES, the transition metal ratio was not changed significantly by the coating processes (Table S1). With increasing Al content, the

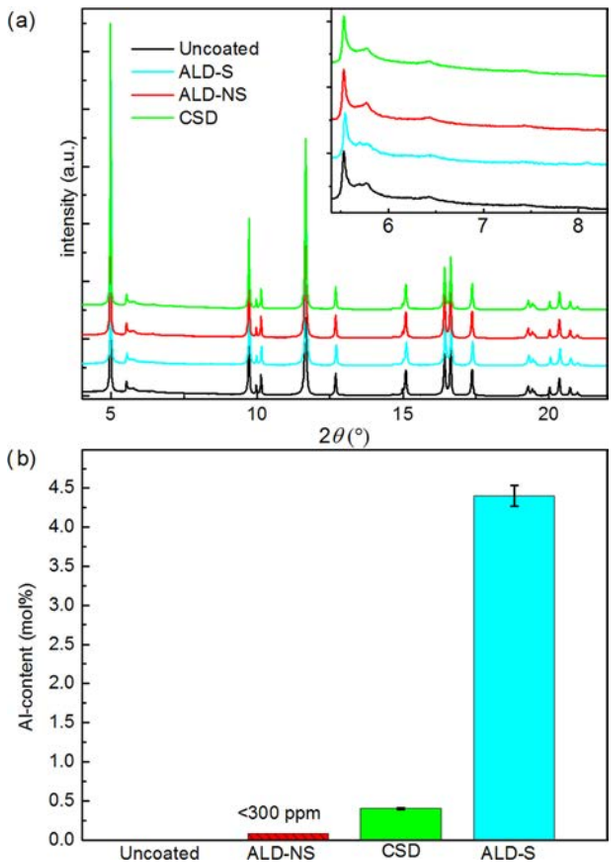

Figure 2. (a) Synchrotron radiation powder diffraction patterns and (b) Al content in mol % measured by ICP OES for the given samples.

amount of Ni, Co, and Mn decreases proportionally. The Li^+ content decreased after the powders were treated by different coating procedures, as reported by Wen et al.[3] This is explained either by Li^+/H^+ exchange caused by the water vapor used for the ALD treatment or by dissolution of the Li ions in the ethanol for the wet coating process. Han et al.[6] showed by ^{7}Li MAS NMR for a wet coating process using water as solvent that such an exchange of cations can occur. Figure 2b illustrates the Al content: the Al content of the CSD sample was close to the target composition: 0.4 mol % Al corresponds to approx. 0.5 wt % aluminum oxide. The Al content for ALD NS could not be quantified precisely due to a small sample amount and very low Al content (of less than 300 ppm). Although both sets of parameters for coating were adjusted to a target thickness of 2−3 nm, the ALD S sample shows the highest Al content, which corresponds to 5 wt % aluminum oxide, so more alumina is deposited than that for the ALD NS sample.

SEM pictures of the uncoated and coated particles can be found in Figure S3. The overall morphologies of all powder samples are similar, generally revealing the existence of agglomerates. This is in agreement with results of Lee et al.[16] who also synthesized $Li_{1.2}Ni0_{.15}Mn_{0.55}Co_{0.1}O_2$ by a sol−gel synthesis.

On the micrometer resolution, the uncoated and the CSD samples display loosely or even nonagglomerated primary particles (agglomerate size $\leq$ 1 μm). On the contrary, both ALD treated samples show agglomeration into secondary particles with sizes between 20 and 80 μm. This agglomeration is caused either by a kind of gluing of the particles by the alumina or by processing the powders in the ALD reactor. Due to the low Al concentration of the ALD NS sample, the ALD process itself is supposed to be responsible for agglomeration. Possibly, the water vapor and nitrogen flow through the powders enhance agglomeration. The water might modify the surfaces and thus facilitate the agglomeration of adjacent primary particles. As described by Bockholt and Indrikova,[17] the secondary particle size might indirectly influence processing of the composite cathodes and thus the electro chemical properties. For example, a higher surface area might cause a higher necessary amount of conductive carbon to achieve the same electronic conductivity by covering a sufficient amount of the particles' surfaces.

On the sub micrometer resolution, SEM mainly shows primary particles with sizes between 100 and 400 nm and sharp edges for all samples (see Figure S3). Some particles are even smaller (approx. 10 nm) due to the ball milling. No significant differences concerning particle sizes and morphol ogy can be observed for the uncoated and the coated particles.

3.3. Estimation of Coating Thickness Based on Specific Surface Area Determined by Gas Adsorption and ICP-OES Results. The obtained uncoated powder exhibits a specific surface area of 14 m^2/g after ball milling, determined by gas adsorption, which is just slightly higher than that of other Li rich NCM powders (10 m^2/g[18]). The BET model implies no chemical interaction between nitrogen and the measured powder. The results of Qiu et al.[19] indicate that some gases interact with Li rich NCM. This could probably lead to an overestimation of the measured specific surface area determined by gas adsorption, resulting in an underestimation of the estimated thickness of the coating.

Sol−gel synthesis yields no spherical secondary structure, as observed for co precipitation synthesis, and might thus always result in higher surface areas. Additionally, the surface area was increased by the applied ball milling step. Taking into account the measured specific surface area, the ICP OES results, and the typical density of alumina (approx. 4 g/cm^3), this would give a theoretical coating thickness of about 0.1 nm for an alumina concentration of 0.5 wt % and a uniform coating for the CSD sample. As shown by the previously measured alumina coated Si wafers, a mixed signal of bulk (manganese) and coating material (aluminum) is expected for such a thin coating in ToF SIMS spectra.

Calculating the theoretical thickness based on the values of specific surface area and alumina concentration given by Wen et al.[3] leads to a theoretical thickness of around 3 nm for their samples. Nevertheless, the effect on the electrochemical properties reported in the present work and ref 3 is very similar. Despite the huge differences of theoretical coating thickness, both studies reveal a stabilization of capacity retention. As will be described in more detail below, the coating process itself has a considerable effect on the electrochemical properties.

3.4. Lateral Coverage Analysis Using ToF-SIMS. In contrast to SEM/EDX, ToF SIMS provides a very high surface sensitivity of a few nanometers. In combination with the possibility to scan large areas in the millimeter range by so called stage raster scans, information about the degree of coverage with a very high lateral resolution can be easily obtained.

3.4.1. ALD Alumina-Coated Si Wafer as a 2D Model System. Two reasons, caused by instrumental and sample restrictions, make it impossible to retrieve information about

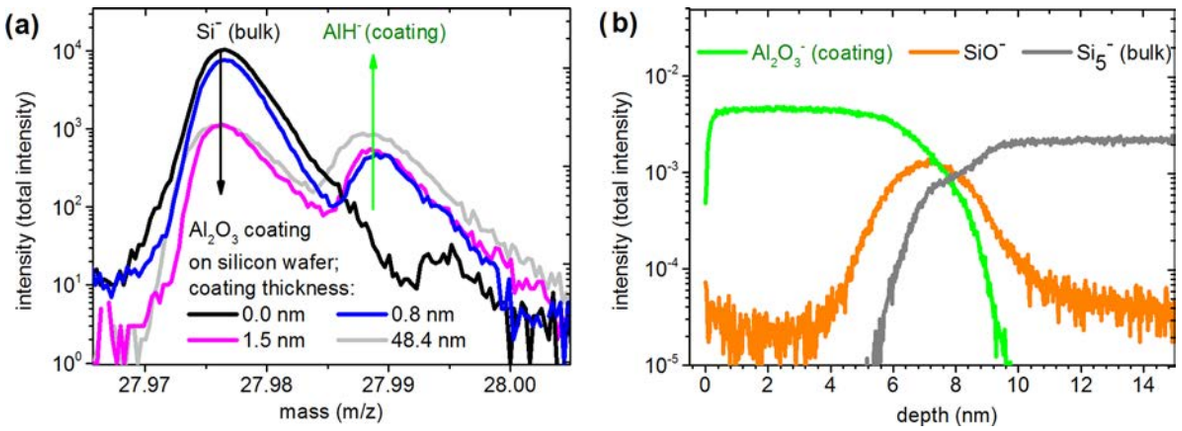

Figure 3. ToF SIMS analysis of silicon wafers coated with different coating thicknesses: (a) Comparison of spectra of 0.0 nm (black), 0.8 nm (blue), 1.5 nm (pink), and 48.4 nm (gray) alumina ALD coating on silicon wafers. Coating layer impurity level of Si is reached at 1.5 nm coating thickness. (b) Depth profile of a coated wafer (5.5 nm) showing the measurement depth sensitivity.

the powder surface by depth profiling directly: During the sputtering process performed to obtain depth profiles the particles are electrostatically charged, which prevents con tinuous measurement. In addition, topographical effects of powder particles influence and broaden the signals, respec tively, and thus complicate the interpretation of the results of the measurement.

To determine the detection limit corresponding to a full coverage of the coating, a 2D model system was investigated by ToF SIMS. Flat silicon wafers as a well defined, two dimen sional, flat substrate were used as a reference. They were coated by ALD with aluminum oxide with various thicknesses (0.0, 0.2, 0.8, 1.3, 1.5, 1.9, 2.8, 5.5, and 48.4 nm). The thicknesses were measured by ellipsometry. Figure 3a shows the measured ToF SIMS spectra with negative polarity of selected wafers measured with the same parameters as those used for the stage raster scans of the different powder materials. The complete set of measurements is shown in Figure S4. The Si^- and AlH^- peaks are very close to each other, but due to the high mass resolution of the high current mode, discrimination is possible.

With increasing coating layer thickness, the Si^- signal approaches a constant value giving the silicon impurity level of the coating layer. The AlH^- signal increases and broadens continuously with increasing coating thickness probably due to a higher ionization probability caused by a higher available "bulk coating" amount. For this reason, the Si^- signal can serve as an indicator for the determination of the detection limit of full coverage. The Si^- signal of the sample with a 1.5 nm thick coating and that of the sample with the thickest coating are nearly identical. This convergence to the bulk impurity level indicates the minimal thickness for which an alumina covered surface shows no bulk signal anymore. The proposed way of estimating coating thicknesses with just surface analysis by calibration of different layer thicknesses of the coating therefore is a good solution if sputtering is not possible due to experimental constraints. Even a closed and homogenous coating with a thickness of less than 1.5 nm causes a mixed signal in the ToF SIMS measurement that might be interpreted as a nonclosed coating.

In Figure 3b, the depth profile of a 5.5 nm coated silicon wafer is presented, which confirms that ToF SIMS can achieve a depth resolution of a few nanometers.

3.4.2. Powder Analysis Using Stage Raster RGB Overlays To Present the Al Distribution with Micrometer Resolution. At first, reference materials made of pure Al_2O_3 and uncoated cathode active material (CAM) were compared as shown in Figure 4 by so called red green blue (RGB) overlays (pixel size

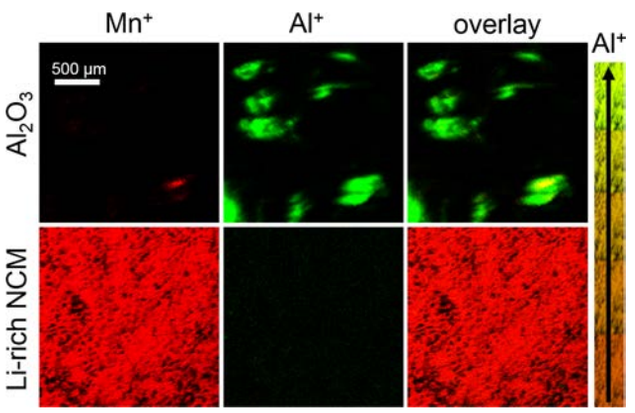

Figure 4. ToF SIMS surface images obtained with the stage raster mode. Measurements were performed in positive polarity, detecting the signal intensity distribution of Mn^+ and Al^+ (single charged secondary ions) for a 2 mm × 2 mm area for reference materials. The magnification given in the top left image is used for all figures. For direct comparison, the overlay of the secondary ion signals (Al^+ in green, Mn^+ in red) is shown in the third column. The arrow indicates the color change of the overlay picture with increasing coating layer intensity and decreasing signal intensity of the cathode material; upper row: pure Al_2O_3, lower row: pure cathode active material $Li_{1.2}Mn_{0.55}Ni_{0.15}Co_{0.1}O_2$.

of about 5 × 5 μm^2). These overlay pictures can be reduced to two colors just using red and green, for example, to give a better contrast for the comparison of two different ToF SIMS signal intensities. In this study, the distribution of covered (Al^+ signal intensity) and uncovered CAM (Mn^+ signal intensity) is shown. As expected, the pure coating material shows high Al^+ signals, which are mapped in green. Pure CAM shows high Mn^+ signals, which are mapped in red with nearly no contamination. In the case that a signal from Al^+ (red) and Mn^+ (green) originates from the same spot of the material, the correspondent overlay indicates this by a yellow color coding (Figure 4 on the right).

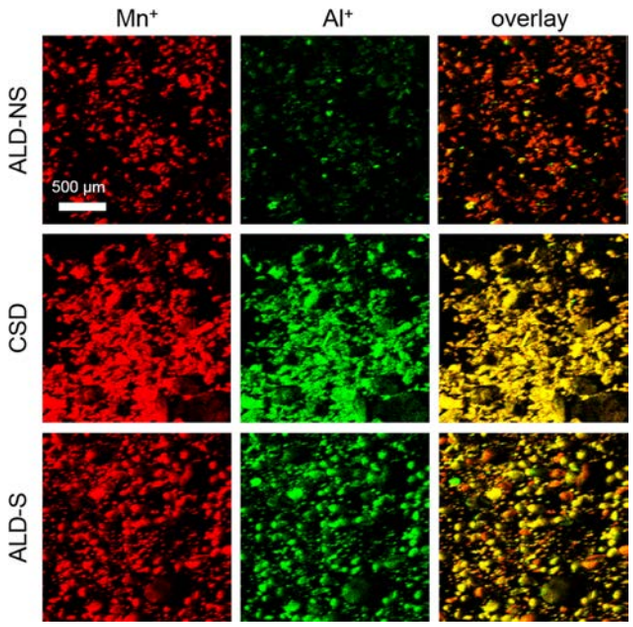

Figure 5. ToF SIMS surface images obtained with the stage raster mode. Measurements were performed in positive polarity detecting the signal intensity distribution of Mn^+ and Al^+ (single charged secondary ions) for a 2 mm × 2 mm area for ALD NS, CSD, and ALD S. The magnification given in the top left image is used for all figures. For direct comparison, the overlay of the secondary ion signals is shown in the third column.

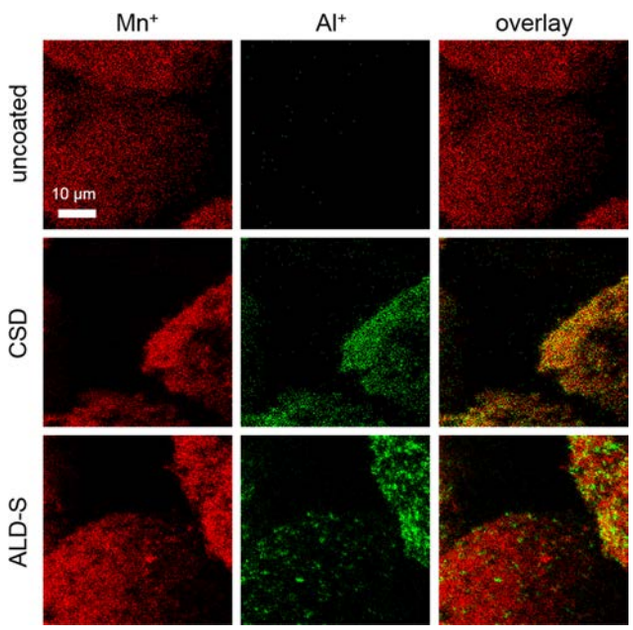

Figure 6. ToF SIMS surface images recorded with delayed extraction mode. Measurements were performed in positive polarity, detecting the signal intensity distribution of Mn^+ and Al^+ (single charged secondary ions) for the uncoated, CSD, and ALD S sample. The magnification given in the top left image is used for all figures. For direct comparison, the overlay of the secondary ion signals is shown in the third column.

ToF SIMS stage raster measurements give a good overview of the coverage over a large investigated area (several mm^2), with a resolution on the micrometer scale for the used powder samples. The overview stage raster ToF SIMS in Figure 5 compares the different coatings in red green overlay mappings. The Mn^+ signal in red as a marker ion for the bulk material and the Al^+ signal reveal huge differences for the coatings. All coatings show Mn^+ signals, indicating that no surface is completely covered with the coating material with a thickness of at least 1.5 nm.

For the ALD NS sample, a few particles show quite strong Al^+ signals but most particles show very weak or nearly no Al^+ signal at all. However, the huge manganese intensities are quite large over the complete sample. In contrast, the ALD S powder shows many agglomerates with a high Al content. There is a strong correlation between the coating and bulk signals, although local variations of the Al^+ signal strength on neighboring agglomerates are visible. The CSD sample shows a high correlation between the Mn^+ and Al^+ signals and a quite homogenous color in the RGB overlay image. Here, a more homogenous distribution of the aluminum on the particle's surface is achieved compared with all other samples.

However, high intensities of transition metal signals can be detected for all samples. This indicates that completely dense coatings with thicknesses larger than 1.5 nm do not exist. There are at least three different possibilities to interpret these mixed signals of aluminum and transition metals: (i) Island grown alumina, (ii) homogenous but thinner coatings, or (iii) homogenous doping into the surface region. Additionally, the CSD and ALD S samples were investigated with the delayed extraction mode of the ToF SIMS instrument to resolve more details of the particle's surface. This allows determining the Al distribution with higher lateral resolution for a smaller lateral area of the sample.

3.4.3. Powder Analysis with Higher Lateral Resolution Using Delayed-Extraction Mode RGB Overlays. Delayed extraction imaging with ToF SIMS offers a lateral resolution down to 100 nm. In the images in Figure 6, pixel size is 200 × 200 nm^2. In this way, details of the particle's surface in the range between those on the micrometer resolution of an overview spectra and TEM resolution (nanometers) can be obtained. Both, the CSD and ALD S sample, show a high Mn and Al correlation for the measured ToF SIMS stage raster (see Figure 5). As shown in Figure 6, it is possible to reveal differences between these two samples concerning their aluminum and transition metal contribution with a higher lateral resolution by delayed extraction imaging.

The CSD sample has a homogenous distribution of Al within this resolution, confirming the results of the stage raster mode. In contrast, it becomes obvious at this resolution that the ALD S sample surface is coated inhomogenously and seems to consist of small Al enriched islands. These Al rich islands spread across the surface with varying number of islands for different agglomerates. The inhomogeneities at this resolution cause the variation of colors for neighboring agglomerates for the stage raster measurements for the ALD S sample (see Figure 5).

3.5. Local Coverage Analysis Using TEM and STEM-EDX Line Scans. Figure 7 shows the S/TEM dark field images for the uncoated (a) and various coated (b–d) materials. The corresponding EDX line scans are shown in Figure 7e–h. TEM bright field images for the uncoated and various coated materials are shown in the Supporting Information (Figure S5). The uncoated material shows lattice fringes with 0.47 nm spacing, which are visible up to the edge of the particle in the TEM bright field image. This distance corresponds to the (003) plane of the layered structure ($R3m$)

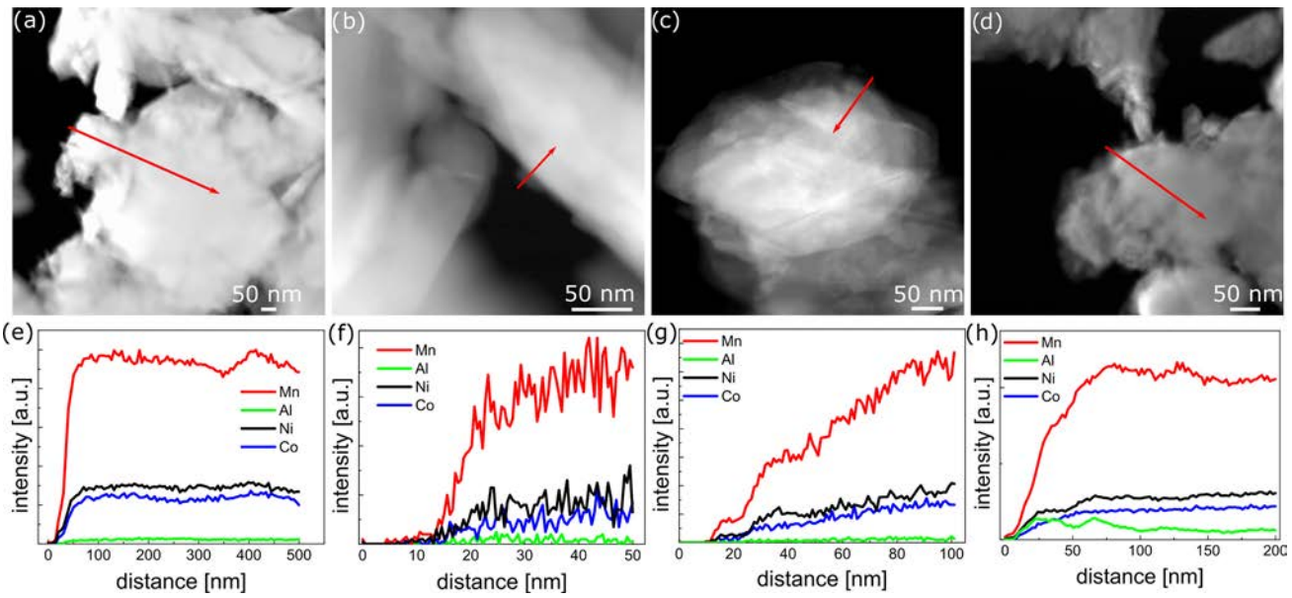

Figure 7. STEM dark field images with position of EDX line scan (a–d) and corresponding line scans (e–h): (a, e) uncoated powder, (b, f) CSD, (c, g) ALD NS, and (d, h) ALD S.

and is in good agreement with the measured synchrotron powder diffraction data. There is no hint of a surface layer on top of the particles.

Before comparing the different coating modifications it has to be mentioned that for all coated samples also, particles with no indication of a coating were found with S/TEM. In accordance with the ToF SIMS results, this leads to the conclusion that none of the powder surfaces were densely and homogenously coated.

The S/TEM EDX line scan (Figure 7f) of the CSD sample displays mainly the signals of Mn, Ni, and Co, whereas the Al signal is very weak. A clear indication for the presence of Al is obvious by EDX mapping (Figure S6), which shows a homogenous Al, Mn, Ni, and Co distribution over the selected area. The very low Al signal intensity corresponds to the amount determined from ICP OES elemental analysis. However, Figure S5b shows particles with a brighter, irregular feature in the surface region.

S/TEM EDX line scan for the ALD NS sample (Figure 7g) also shows a weak intensity of Al signal, indicating the presence of a coating. Particles with an amorphous outer shell characterized by a brighter contrast were found (Figure S5c). A weaker contrast compared to the transition metal containing bulk material might be caused by lighter elements such as C or Al. This material is characterized by a high beam sensitivity, hampering reliable EDX analysis. In the Supporting Information, the investigated area is shown before and after EDX measurement (Figure S7).

The ALD S sample contains the highest Al amount measured by ICP OES. This is in good agreement with S/TEM EDX line scan (Figure 7h). The variation of the Al signal shows that even for this sample, the coating is not homogenous in all areas. The line scan originates from the area shown in Figure S5d but tilted 20° toward the EDX detector, with lower magnification. The particle indicated by the red line in Figure S5d, lying like an island on top or below the matrix material, has a high Al content, as shown in Figure 7h. Lattice fringes of the bulk material do not reach the edge of the particle (Figure S5d). An approximately 3–5 nm thick, amorphous appearing layer is found on the surface. This is highlighted in the magnified inset (Figure S5d). Zhang et al.[5] also proposed to use 2–3 nm thick alumina coatings on Li rich NCM and reported increased capacity retention.

Without information about elemental composition, the morphologies seen in the TEM images were interpreted as "coated surfaces" for all three modifications. All images show either amorphous surfaces or at least a weaker surface contrast compared with the bulk. Therefore, a different surface structure is visible. EDX line scans on different areas display that only the ALD S sample surface shows an Al enrichment characteristic of a coating on the surface. The CSD sample shows evidence for a homogenous Al distribution (EDX maps), which could be interpreted as a coating. The very homogenous Al distribution was confirmed by ToF SIMS on various resolutions. However, in the edge area, enrichment of aluminum could not be detected by EDX line scans with TEM.

3.6. Brief Discussion of the Powder Characterization.

Taking all investigations described so far into account, a large variety of the appearance of the different coating modifications on different length scales was found. Only with the combination of analysis methods operating with different resolutions it was possible to clearly differentiate between the degrees of coverage of the coatings. It was shown that no sample was homogenously and completely covered by a coating. Island growth on different powder particles was identified for ALD S, a nonuniform coating distribution for ALD NS, and a surface modification that rather can be considered as a kind of surface doping for the CSD sample.

Because none of the powders that were supposed to be coated possess a dense, homogenous thin coating phase on their surface, the improvements concerning initial capacity and/or capacity retention are supposed to be induced by one of the following points or a combination of them: the process itself, the alumina acting as an additive, e.g., for HF scavenging or a reduced effective cathode material surface area by a coating.

3.7. Experiments To Check Considerable Influence of the Process Used for the Wet Coating and the Addition

of Alumina as Powder Mixture. To differentiate effects occurring for the CSD sample from those caused by the coating process itself and those caused by the addition of alumina to the material system as a powder mixture, dedicated experiments were conducted. For the powder mixture reference sample, alumina was produced by the synthesis route used for the wet coating process but without the Li rich NCM. Electrochemical cells containing a powder mixture of 0.5 wt % of this material and uncoated Li rich NCM as cathode material served as reference to demonstrate how the addition of alumina affects the electrochemical properties without forming a coating (sample "Mix"). For the process reference sample, the wet coating process of the base Li rich NCM material was performed without using the $Al(NO_3)_3$ precursor (sample "Proc"). Figure 8 compares the evolution of the specific discharge capacity in full cells for the uncoated sample, CSD, Mix, and Proc.

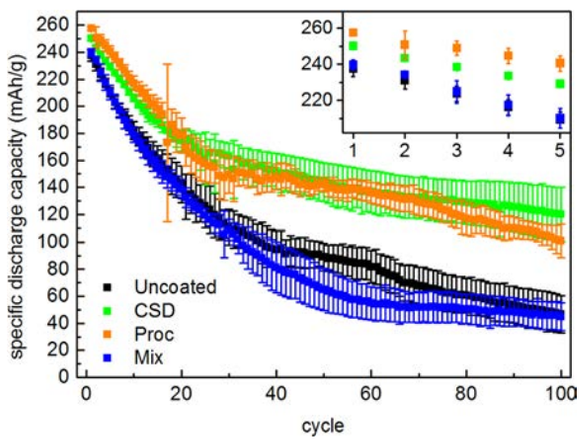

Figure 8. Evolution of discharge capacity for a process reference Proc (orange) and powder mixture reference Mix (blue) compared with the CSD sample (green) and uncoated sample (black), 100 cycles in full cells vs graphite anode between 2.0 and 4.7 V at a rate of approx. C/10 are shown; mean values and standard deviation are determined for 4–6 cells.

The comparison of the Mix sample and the uncoated powder (see Figure 8) reveals that the use of 0.5 wt % alumina in a powder mixture used for the cathode composite electrode did not change the specific discharge capacity significantly. Using 10 times more commercial, nanosized Al_2O_3 powder as an additive for HF scavenging and blending it with the other electrode constituents of the positive electrode, Bettge et al.[20] found improved capacity retention for this material system.

Compared with the uncoated powder, the CSD sample, as well as the Proc sample, displays improved electrochemical properties. The Proc sample shows a higher initial capacity and capacity retention than those of the uncoated material, similar to the effect obtained by the wet coating for the CSD sample. The process alone seems to cause a near surface structural change, which might be responsible for the improved electrochemical properties. It is mandatory to include process reference samples to clearly separate effects on electrochemical properties originating exclusively from particle coating from sample modifications induced only by the process itself.

3.8. Discussion. The coating characteristics derived from the powder analyses are illustrated schematically in Figure 9. The uncoated sample, CSD sample, and process reference sample consist of just little agglomerated or loose primary particles, whereas the ALD treated powders formed secondary agglomerates with more than 10 μm diameter, as described in more detail in the SEM section. The powders that were not treated by the ALD process preserve the loose primary particle structure as obtained by the sol–gel synthesis. Thus, they might need more conductive carbon to form sufficient conductive pathways compared with the secondary agglomerated structures. Since a very high amount of conductive carbon (6 wt % C65) was used for slurry preparation, it is assumed that all examined powders had sufficient content of conductive carbon to ensure proper electrochemical contribution of all particles.

The powder analysis of the coated surfaces gave another turn to the interpretation of the electrochemical data, as described in the literature. Since none of the powders showed a complete, thick, and dense coating, the electrochemical data must be interpreted with caution. There is very fast capacity degradation for all of the samples. Even those with the highest

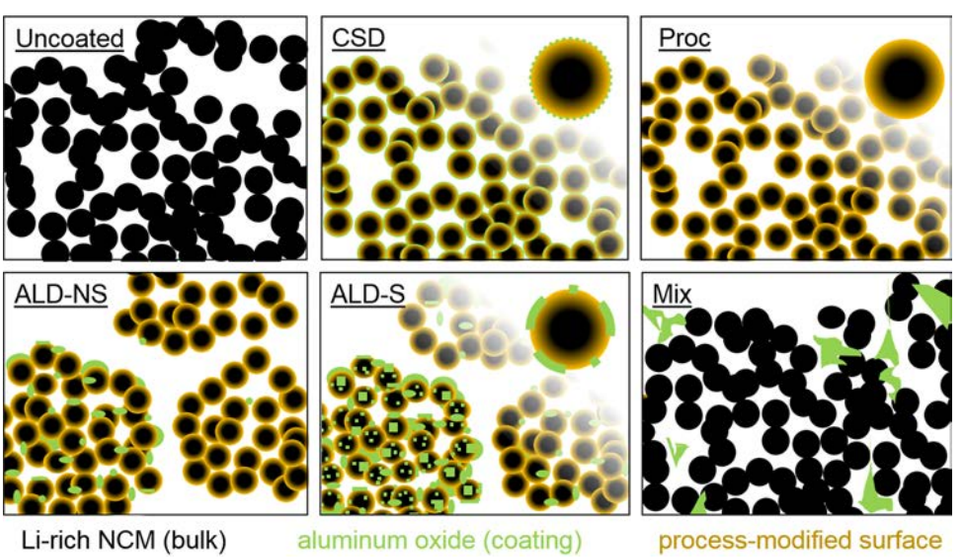

Figure 9. Scheme summarizing the results of the surface analytical techniques for all samples (not drawn to scale).

capacity retention lost about 25% of their initial specific discharge capacity after 20 cycles. The fast degradation is due to the high surface area of the powders. This indicates that surface degradation processes represent a large portion of the capacity loss occurring in this material system. They cannot be overcome completely by all applied coating processes.

For the ALD S sample, an aluminum signal could be detected by ToF SIMS over almost the whole analyzed surface area with varying signal intensities from particle to particle agglomerate. This sample displayed many islandlike Al containing coated surfaces. The initial capacity decreased by about 30% compared to that of the uncoated material, although the complete amount of alumina in the powder was only about 5 wt % (determined by ICP OES). This large nonlinear decrease of specific discharge capacity in the first cycle supports the passivation of particle surfaces due to a coating. The island type thick coatings, as experimentally proven to exist for this material, are supposed to block or to considerably lower the Li diffusion for a significant part of the interface between electrolyte and active material, respectively. A poor electronic contact might also decrease the rate capability. As a consequence, the activation process in the first cycle might be slowed down. The process is supposed to be related to oxygen release at the surface and plays a crucial role for Li rich NCM materials. It might not be completed after the first cycle but is prolonged for many cycles. In addition to a slower Li diffusion, an inactivation of particles due to blocked active material regions is possible. This hypothesis is supported by the charge−discharge curve shown in Figure 1d that appears compressed compared to that of the uncoated sample on the specific capacity axis. These two aspects can explain why the ALD S sample starts with a quite low initial capacity but exhibits improved cycling stability compared to that of the uncoated material.

The ToF SIMS stage raster scans obtained for the ALD NS powder demonstrate that only few agglomerates possess a high aluminum content whereas for other agglomerates, no aluminum contribution was detected. The elemental analysis indicates very low Al content. Nevertheless, a significant improvement of its electrochemical properties was found. The specific discharge capacity of the first cycle is improved by 7% in half cells and by 4% in full cells. As shown by the sample ALD S, it is not beneficial for the initial capacity when a majority of particles are coated with a thick and at least partially closed coating by ALD. Since only a comparable small number of particles of ALD NS sample exhibit a kind of island grown coating, there is also a small effect of the coating on electrochemical performance as a consequence. So it is more reasonable that the increase of the initial capacity for the ALD NS sample results from modifications at a high fraction of the surface area than from a low fraction of the overall surface area modified by the coating. The majority of the particles were probably modified by the ALD process itself. An influence of the process by contact with water vapor or nitrogen at elevated temperature would affect a high number of particles even in the case of insufficient available precursor amounts, retention time, and/or insufficient mixing.

The CSD sample was apparently not coated with a thick and dense coating at all, as revealed by the analytical investigations presented here, but still exhibits the most promising improvement of its electrochemical properties. A homogenous Al distribution does not necessarily mean that there must be a covering surface coating. The very homogenous distribution of Al on multiple scales rather supports the following models: (i) an extremely thin and homogenous coating, (ii) a doping of the cathode active material oxide particles, or (iii) a segregation of Al on grain boundaries. Dogan et al.[21] have shown via ^{27}Al NMR for a formally Al doped NCM that there are no transition metals next to nearest neighbors around Al. They conclude that there is a repulsion between Mn and Al ions for this material and no doping occurs. Thus, a doping of Li rich NCM (with a high manganese content) with Al might be improbable but rather a segregation into the grain boundaries occurs. Nevertheless, Li rich NCM shows a behavior different from that of conventional NCM due to the different crystal structures, including integrated Li_2MnO_3 domains, and could enable doping in this way.

As shown with the reference experiments using a process and powder mixture references, even the process itself causes an improvement of the electrochemical properties. It is still not clear whether the contact with the liquid solvent, the subsequent calcination, or a combination of both causes a modification of the surface. Wen et al.[3] reported a delithiation of about 8 mol % by a similar wet coating using aluminum nitrate and water instead of ethanol and found a spinel reflection in their diffraction data when they calcined their sample at 500 °C. In a similar way, the wet coating process causes a structural rearrangement of the first few nanometers of the material due to transformation from layered to spinel. The transformation is caused by a delithiation or dissolution of lithium from the particles' surfaces during the ethanol treatment and subsequent calcination. This explanation is supported by the appearance of the 2.7 V peak in the first differential capacity plot, which is attributed to a spinel like structure.[3] ICP OES exhibits a significant Li loss of about 6 mol % for the wet coated sample, which supports the hypothesis for the formation of a spinel. Conversely, Xu et al.[2] claim to suppress a layer to spinel transformation and find no evidence for a spinel surface modification when they applied sol−gel coating using aluminum isopropoxide and water in ethanol as solvent with a calcination temperature of 500 °C as well.

Another possible mechanism would be the reduction of surface carbonates: As reported by Jung et al.,[22] carbonates might form on the surface when transition metal oxide based cathode materials are stored under ambient conditions. Probably, the carbonate concentration on the surface is decreased by the wet process. This decrease could, in a second step, decrease the electrolyte oxidation.[23] To clarify the underlying mechanism further, experiments are needed.

Many publications have reported of a beneficial effect on electrochemical performance by coatings on Li rich NCM.[2−5] However, throughout these works, there is a large variation concerning the thicknesses of the coatings with respect to theoretical predictions as well as experimental values. From the specific surface area determined by gas adsorption and amount of coating material obtained by ICP OES, it is possible to calculate an average coating thickness. By comparison of the thicknesses measured by TEM and these calculated values, it is possible to evaluate the homogeneity of a coating.

The presented results show that this homogeneity and also the influence of the coating process itself has a strong influence on electrochemical properties. Han et al.[6] compared a process reference using water as solvent for a coating process on conventional NCM with the uncoated material and found no indication for an influence. Potentially, the process influence

on Li rich NCM caused by the ethanol treatment and calcination used in this work is a little different from the work described by Han et al.:[6] The overlithiation might cause a higher tendency to dissolve Li ions from the surface lattice, and thus structural rearrangements could take place during calcination. Additionally, if oxygen contributes to the activation process of Li rich NCM on the surfaces,[12] there would be a higher sensitivity for surface modifications as well. Further investigations, including treatment with acids[24] or alcohols, e.g., ethanol, at various temperature treatments could be used to examine the influence of various wet chemical treatments on the electrochemical properties. It might be possible that many studies describing the influence of a coating are rather influenced by process steps during material preparation. The experiments strongly indicate that a process reference is necessary to consider process influences.

Additionally, it is necessary to analyze the coverage and distribution of the coating material on the surface on different length scales to reveal the correlation between underlying composite structures and resulting electrochemical properties, such as initial capacities and capacity fade.

4. CONCLUSIONS

In this study, the surface analysis of differently coated cathode active material particles with micrometer and nanometer resolution was presented. By using S/TEM EDX and ToF SIMS, it was possible to reveal differences in the coverage homogeneity for the three coating techniques. Especially, ToF SIMS surface analysis proved to be very versatile for the analysis of the coating homogeneity on large areas but still with a very high surface sensitivity. It was shown that even the ALD treated powders ALD S and ALD NS exhibited uncovered transition metal oxide surfaces. An island growth instead of a dense alumina coating layer was observed. None of the samples is fully covered by a dense coating layer, although all coating techniques cause an increase of capacity retention. For the ALD NS and CSD sample, even an increase of the initial capacity was observed.

No clear improvement of the electrochemical properties correlated with an increasing degree of coverage (comparison of ALD NS with ALD S) was found. In summary, no obvious dependence of the degree of coverage on the electrochemical properties was found. Samples with added alumina as powder mixture do not significantly vary from the uncoated sample. In contrast to other studies, our approach to include the investigation of a process reference sample is a step forward for a better understanding of coating processes on cathode active materials. The uniform distribution of aluminum on different length scales for the CSD sample was not decisive for the improvements in the electrochemical properties of this sample. Instead, it was shown that already the coating process itself likely causes the improvement of the initial capacity and capacity retention, as seen for the CSD sample.

In contrast, the ALD S sample has a high concentration of alumina islands on the particle agglomerates. This leads to a significant partial coverage of the surfaces, which causes the starting capacity to drop by about 30%. This means that the effects of the coating coverage and the process influence overlap. The partial coverage decreases the capacity, whereas the process influence increases the retention of the capacity.

AUTHOR INFORMATION

Corresponding Author

*E mail: nadine.dannehl@partner.kit.edu.

ORCID

Nadine Dannehl: 0000 0002 0733 6610

Sylvio Indris: 0000 0002 5100 113X

Present Address

[‖]Left KIT on 2018 02 28, now at VDE Renewables GmbH, Siemensstraße 30, D 63755 Alzenau, Germany (S.O.S.).

Author Contributions

The manuscript was written through contributions of all authors. All authors have given approval to the final version of the manuscript.

Notes

The authors declare no competing financial interest.

ACKNOWLEDGMENTS

The authors acknowledge Robert Bosch GmbH for financial support. Finally, the support for ALD coatings, TEM, and ToF SIMS measurements by the Karlsruhe Nano Micro Facility (KNMF, http://www.knmf.kit.edu/), a Helmholtz research infrastructure at the Karlsruhe Institute of Technology (KIT), is gratefully acknowledged. Beamtime allocation and staff support at beamline BL04 MSPD at the ALBA Synchrotron in Barcelona, Spain, is gratefully acknowledged. This work contributes to the research performed at CELEST (Center for Electrochemical Energy Storage Ulm Karlsruhe).

REFERENCES

(1) Croy, J. R.; Balasubramanian, M.; Gallagher, K. G.; Burrell, A. K. Review of the US Department of Energy's Deep Dive Effort to Understand Voltage Fade in Li and Mn Rich Cathodes. *Acc. Chem. Res.* **2015**, *48*, 2813−2821.

(2) Chen, Z.; Xu, M.; Li, L.; Zhu, H.; Zhao, Q.; Xu, L.; Peng, N.; Gong, L. Highly Crystalline Alumina Surface Coating from Hydrolysis of Aluminum Isopropoxide on Lithium Rich Layered Oxide. *J. Power Sources* **2015**, *281*, 444−454.

(3) Wen, X.; Liang, K.; Tian, L.; Shi, K.; Zheng, J. Al_2O_3 Coating on $Li_{1.256}Ni_{0.198}Co_{0.082}Mn_{0.689}O_{2.25}$ with Spinel Structure Interface Layer for Superior Performance Lithium Ion Batteries. *Electrochim. Acta* **2018**, *260*, 549−556.

(4) Park, M. S.; Lee, J. W.; Choi, W.; Im, D.; Doo, S. G.; Park, K. S. On the Surface Modifications of High Voltage Oxide Cathodes for Lithium Ion Batteries: New Insight and Significant Safety Improvement. *J. Mater. Chem.* **2010**, *20*, 7208.

(5) Zhang, X.; Belharouak, I.; Li, L.; Lei, Y.; Elam, J. W.; Nie, A.; Chen, X.; Yassar, R. S.; Axelbaum, R. L. Structural and Electrochemical Study of Al_2O_3 and TiO_2 Coated $Li_{1.2}Ni_{0.13}Mn_{0.54}Co_{0.13}O_2$ Cathode Material Using ALD. *Adv. Energy Mater.* **2013**, 1299−1307.

(6) Han, B.; Paulaukas, T.; Key, B.; Peebles, C.; Park, J.; Klie, R.; Vaughey, J. T.; Dogan, F. Understanding the Role of Temperature and Cathode Composition on Interface and Bulk: Optimizing

Aluminum Oxide Coatings for Li Ion Cathodes. *ACS Appl. Mater. Interfaces* **2017**, *9*, 14769−14778.
(7) Zhang, L. L.; Chen, J. J.; Cheng, S.; Xiang, H. F. Enhanced Electrochemical Performances of LLMO Cathode Materials by Coating $LiAlO_2$ for Lithium Ion Batteries. *Ceram. Int.* **2016**, *42*, 1870−1878.
(8) Brunauer, S.; Emmett, P. H.; Teller, E. Adsorption of Gases in Multimolecular Layers. *J. Am. Chem. Soc.* **1938**, *60*, 309−319.
(9) Rietveld, H. M. A Profile Refinement Method for Nuclear and Magnetic Structures. *J. Appl. Crystallogr.* **1969**, *2*, 65−71.
(10) Bloom, I.; Trahey, L.; Abouimrane, A.; Belharouak, I.; Zhang, X.; Wu, Q.; Lu, Q.; Abraham, D. P.; Bettge, M.; Elam, J. W.; Meng, X.; Burrell, A. K.; Ban, C.; Tenent, R.; Nanda, J.; Dudney, N. Effect of Interface Modifications on Voltage Fade in $0.5Li_2MnO_3{\bullet}0.5LiNi_{0.375}Mn_{0.375}Co_{0.25}O_2$ Cathode Materials. *J. Power Sources* **2014**, *249*, 509−514.
(11) Nayak, P. K.; Grinblat, J.; Levi, M.; Levi, E.; Kim, S.; Choi, J. W.; Aurbach, D. Al Doping for Mitigating the Capacity Fading and Voltage Decay of Layered Li and Mn Rich Cathodes for Li Ion Batteries. *Adv. Energy Mater.* **2016**, No. 1502398.
(12) Armstrong, A. R.; Holzapfel, M.; Novak, P.; Johnson, C. S.; Kang, S. H.; Thackeray, M. M.; Bruce, P. G. Demonstrating Oxygen Loss and Associated Structural Reorganization in the Lithium Battery Cathode $Li[Ni_{0.2}Li_{0.2}Mn_{0.6}]O_2$. *J. Am. Chem. Soc.* **2006**, *128*, 8694−8698.
(13) Jang, Y. I.; Huang, B.; Wang, H.; Sadoway, D.; Chiang, Y. M. Eletrochemical Cycling Induced Spinel Formation in High Charge Capacity Orthorhombic $LiMnO_2$. *J. Electrochem. Soc.* **1999**, *146*, 3217−3223.
(14) Park, S. H.; Kang, S. H.; Johnson, C. S.; Amine, K.; Thackeray, M. M. Lithium Manganese Nickel Oxide Electrodes with Integrated Layered Spinel Structures for Lithium Batteries. *Electrochem. Commun.* **2007**, *9*, 262−268.
(15) Croy, J. R.; Gallagher, K. G.; Balasubramanian, M.; Long, B. R.; Thackeray, M. M. Quantifying Hysteresis and Voltage Fade in $xLi_2MnO_3{\cdot}(1\ x)LiMnO_{0.5}Ni_{0.5}O_2$ Electrodes as a Function of Li_2MnO_3 Content. *J. Electrochem. Soc.* **2014**, *161*, A318−A325.
(16) Lee, E.; Koritala, R.; Miller, D. J.; Johnson, C. S. Aluminium and Gallium Substitution into $0.5Li_2MnO_3{*}0.5Li(Ni_{0.375}Mn_{0.375}Co_{0.25})O_2$ Layered Composite and the Voltage Fade Effect. *J. Electrochem. Soc.* **2015**, *162*, A322−A329.
(17) Bockholt, H.; Indrikova, M.; Netz, A.; Golks, F.; Kwade, A. The Interaction of Consecutive Process Steps in the Manufacturing of Lithium Ion Battery Electrodes with Regard to Structural and Electrochemical Properties. *J. Power Sources* **2016**, *325*, 140−151.
(18) Streich, D.; Gueguen, A.; Mendez, M.; Chesneau, F.; Novak, P.; Berg, E. Online Eletrochemical Mass Spectrometry of High Energy Lithium Nickel Cobalt Manganese Oxide/Graphite Half and Full Cells with Ethylene Carbonate and Fluoroethylene Carbonate Based Electrolytes. *J. Electrochem. Soc.* **2016**, *163*, A964−A970.
(19) Qiu, B.; Zhang, M.; Wu, L.; Wang, J.; Xia, Y.; Qian, D.; Liu, H.; Hy, S.; Chen, Y.; An, K.; Zhu, Y.; Liu, Z.; Meng, Y. S. Gas Solid Interfacial Modification of Oxygen Activity in Layered Oxide Cathodes for Lithium Ion Batteries. *Nat. Comm.* **2016**, *7*, No. 12108.
(20) Bettge, M.; Li, Y.; Sankaran, B.; Rago, N. D.; Spila, T.; Haasch, R. T.; Petrov, I.; Abraham, D. P. Improving High Capacity $Li_{1.2}Ni_{0.15}Mn_{0.55}Co_{0.1}O_2$ Based Lithium Ion Cells by Modifiying the Positive Electrode with Alumina. *J. Power Sources* **2013**, *233*, 346−357.
(21) Dogan, F.; Vaughey, J. T.; Iddir, H.; Key, B. Direct Observation of Lattice Aluminium Environments in Li Ion Cathodes $LiNi_{1-y-Z}Co_yAl_zO_2$ and Al Doped $LiNi_xMn_yCo_zO_2$ via ^{27}Al MAS NMR Spectroscopy. *ACS Appl. Mater. Interfaces* **2016**, *8*, 16708−16717.
(22) Jung, R.; Morasch, R.; Karayaylali, P.; Phillips, K.; Maglia, F.; Stinner, C.; Shao Horn, Y.; Gasteiger, H. A. Effect of Ambient Storage on the Degradation of Ni Rich Positive Electrode Materials (NMC811) for Li Ion Batteries. *J. Electrochem. Soc.* **2018**, *165*, A132−A141.
(23) Jung, R.; Metzger, M.; Maglia, F.; Stinner, C.; Gasteiger, H. A. Chemical versus Electrochemical Electrolyte Oxidation on NMC111, NMC622, NMC811, LNMO, and Conductive Carbon. *J. Phys. Chem. Lett.* **2017**, *8*, 4820−4825.
(24) Kang, S. H.; Johnson, C. S.; Vaughey, J. T.; Amine, K.; Thackeray, M. M. The Effects of Acid Treatment on the Electrochemical Properties of $0.5Li_2MnO_3{\bullet}0.5\ LiNi_{0.44}Co_{0.25}Mn_{0.31}O_2$ Electrodes in Lithium Cells. *J. Electrochem. Soc.* **2006**, *153*, A1186−A1192.